propanimines with regard to this process.

One can also imagine replacing CH_2, SiH_2, and GeH_2 ring atoms by other groups. This would necessitate only minor changes in our working equation, eq 6. One group of possible replacements worth mentioning is the heavier chalcogens, selenium and telurium. In the last few years, stable M_2Se and M_2Te rings have been synthesized for M = Si, Ge, and Sn.[46] On the other hand, C_2Se rings are unstable, and C_2Te rings have apparently never been made. The origin of the relative stability for the Si, Ge, and Sn rings can be traced to the much weaker π-bonds. In the case of C_2Se and C_2Te rings, the strong π-bond in ethylene provides a significant thermochemical driving force for extrusion of a selenium or telurium atom. In Si, Ge, and Sn rings, this driving force is severely attenuated.

Baines and co-workers[4b] have just reported a fascinating consequence of what our results suggest is a small enthalpy difference in cyclotrimetallane decomposition enthalpies. With the ultimate goal of obtaining a Ge=Si doubly bonded compound, it was decided that the best choice of precursor was a siladigermirane, which it was hoped would decompose according to eq 1 to give the desired germasilene product.[32] Unfortunately, and for unknown reasons, the synthetic route also produced some cyclotrigermane, which could not be separated from the desired precursor by traditional means. It was found, however, that the cyclotrigermane was more thermally labile than the siladigermirane, and the minor component Ge_3 ring was eliminated from the mixture by thermolysis at a reduced temperature. According to our results in Table V for the parent hydride compounds, the cyclotrigermane decomposition has a endothermicity of 47.1 kcal mol^{-1} compared to siladigermirane's 49.7 kcal mol^{-1}. If we assume that the reverse of reaction 1 occurs without barrier so that the endothermicity can be equated with the activation energy, this corresponds to a factor of 40 in the individual rate constants for decomposition at the temperature employed, 80 °C.

Concerning the prospects for synthesizing new cyclotrimetallane rings, we note that the decompositions of $GeSi_2H_6$ and $CSiGeH_6$ are no less endothermic than the decompositions of other rings which have already been synthesized (albeit in highly substituted form), suggesting that $GeSi_2$ and CSiGe rings may be accessible by established synthetic routes. On the other hand, the germirane ring, whose decomposition is ca. 20 kcal mol^{-1} less endothermic than those of any of the other cyclotrimetallanes, clearly presents a greater challenge, and stannirane rings will likely prove even more difficult (vide ante). But if the cyclopropane ring can be destabilized by perfluorination then it ought to be possible to stabilize the germirane ring through judicious substitution for the hydrogen atoms. Replacing the H atoms on Ge with electropositive π-acceptor substituents such as SiH_3 may stabilize the germirane ring by reducing both the ring strain[47] and the DSSE of Ge,[44] although these effects will probably be mitigated by weakening of the Ge-C bonds.[48] Reductions in the C-C π-bond enthalpy (assuming it can be equated with the double bond rotation barrier[25]) of over 20 kcal mol^{-1} can be achieved by placing "push-pull" substituents on the C atoms,[49] and it may be possible to find a pair of these substituents which produce a low C-C π-bond enthalpy without adversely affecting the other contributions to the enthalpy of reaction 1. Thus, the use of carefully chosen substituents is probably the key to the synthesis of germirane and the stabilization of other cyclotrimetallane rings.

Acknowledgment. This research is supported by the Air Force Office of Scientific Research, Grant AFOSR-87-0182. We thank Kim M. Baines for communicating the results of ref 4 prior to publication.

(46) (a) Batcheller, S. A.; Masamune, S. *Tetrahedron Lett.* **1988**, *29*, 3383. (b) Tsumuraya, T.; Sato, S.; Ando, W. *Organometallics* **1988**, *7*, 2015. (c) Tsumuraya, T.; Kabe, Y.; Ando, W. *J. Chem. Soc., Chem. Commun.* **1990**, 1159. (d) Tan, R. P.-K.; Gillette, G. R.; Powell, D. R.; West, R. *Organometallics* **1991**, *10*, 546. (e) Schafer, A.; Weidenbruch, M.; Saak, W.; Pohl, S.; Marsmann, H. *Angew. Chem., Int. Ed. Engl.* **1991**, *30*, 834. (f) Schafer, A.; Weidenbruch, M.; Saak, W.; Pohl, S.; Marsmann, H. *Angew. Chem., Int. Ed. Engl.* **1991**, *30*, 962.

(47) Dill, J. D.; Greenberg, A.; Liebman, J. F. *J. Am. Chem. Soc.* **1979**, *101*, 6814.

(48) Silyl substituents weaken C-C and Si-Si bonds (see ref 11) and thus are expected to weaken Ge-C bonds also.

(49) Sandstrom, J. In *Topics in Stereochemistry*; Allinger, N. L., Eliel, E. L., Wilen, S. H., Eds.; Wiley: New York, 1983; Vol. 14, p 83.

^{27}Al Nuclear Magnetic Resonance Study of Aluminas and Their Surfaces

B. A. Huggins and Paul D. Ellis*

Contribution from the Department of Chemistry, University of South Carolina, Columbia, South Carolina 29208. *Received March 4, 1991*

Abstract: The nature of the surface of α-, γ-, and transition-aluminas has been explored via variable-temperature solid-state ^{27}Al NMR spectroscopy. Results from a previous study of aluminas using ^{27}Al NMR at room temperature showed a loss in signal with increasing surface area. The conclusion based upon these results was that the aluminum atoms in the first two molecular layers of alumina did not contribute to the ^{27}Al NMR signal. Further, the observed signal loss was due to the surface aluminum atoms experiencing a large electric field gradient. Results from the study presented here indicate that a loss in ^{27}Al signal with increasing surface area is real but that it is due instead to dynamic events occurring at the surface. Low-temperature studies served to slow these dynamics, thereby increasing the observable signal by amount greater than expected from the Boltzmann factor alone. We present these data herein and propose mechanisms by which these surface dynamics may occur.

Introduction

Aluminas, general formula Al_2O_3, have been known to have catalytic importance since the late 1700s. Either by themselves, or as supports, the aluminas are responsible for a wide range of catalytic reactions, and the properties of aluminas have been the subject of many investigations.[1] The major emphasis on aluminas today is in their role as supports for metals, mixed-metal oxides, and metal oxides in industrial catalytic processes. The aluminas of choice for these systems are often η- and γ-alumina, with typical respective surface areas of 250 and 220 m^2/g. The surface structure of these and other transition-aluminas is the key to more educated proposals for mechanisms of reactions over these catalytic systems.

What is known about the surface structure of these catalyst supports has resulted from IR studies on surface hydroxyl groups,[2,3]

(1) (a) Tanabe, K. *Solid Acids and Bases*; Academic Press: New York, 1970. (b) Goldstein, M. S. In *Experimental Methods in Catalytic Research*; Anderson, R. B., Ed.; Academic Press: New York, 1968.

(2) Peri, J. B. *J. Phys. Chem.* **1965**, *69* (1), 211.

0002-7863/92/1514-2098$03.00/0

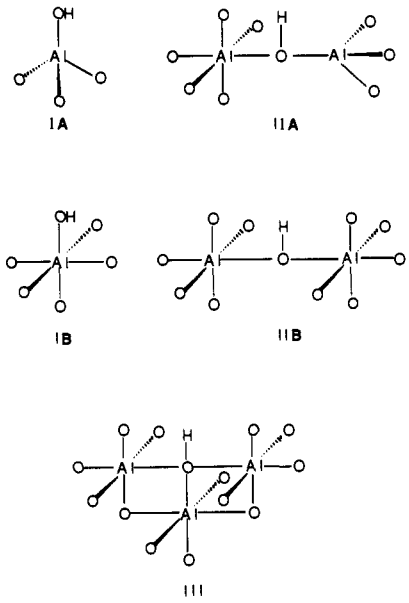

Figure 1. Five types of hydroxyls which have been proposed to exist on the surfaces of γ- and η-aluminas and higher surface area aluminas.

proton[4] and aluminum[5] NMR, and the formation of idealized model systems[6,7] to help interpret what is seen in the IR experiments. There are several features which have been revealed by these studies which have served to lay a foundation for ongoing research. These are (1) the surface of a given alumina is sensitive to the way in which the alumina is prepared,[8] i.e., level of hydration, temperatures, whether or not there is anion activation, etc., (2) IR data suggest that there are five types of hydroxyl groups present on the surface,[3] and (3) the catalytic activity of aluminas requires the presence of defect sites at the surface.[7] These defect sites are areas in which there are two or more adjoining anion vacancies or oxide ions and are created upon dehydroxylating aluminas at temperatures of 400 °C or higher.

There has been a large amount of infrared work done on surfaces in general, and more specifically aluminas, in order to describe and distinguish surface hydroxyls. IR investigations of the surfaces of aluminas have revealed five types of hydroxyl groups.[7] A pictorial representation of these sites is given in Figure 1. As can be seen, there are two types of tetrahedrally coordinated, T_d, aluminum atoms, IA and IIA, and four types of octahedrally coordinated, O_h, aluminum atoms, IIA, IB, IIB, and III. As mentioned, the relative ratios of these sites on any given alumina surface is directly dependent upon the alumina's preparation conditions. The number of combinations of these sites distributed on a given model surface is limited only by one's imagination and available disk space.

The infrared results not only have been helpful in the determination of what types of hydroxyls occur on the surface but also have established guidelines for researchers to use in their models concerning what is not at the surface. There have been several models presented which serve to describe the alumina surface and/or explain the IR spectra of the surface. In Peri's[6] seminal work, he presented a model which uses a single exposed crystallographic plane made up exclusively of a (100) face, containing only octahedrally coordinated aluminum atoms, i.e., a model which should represent the α-alumina surface. Peri described rules for the removal of surface hydroxyls, taking into account the surface energy at each step. The dehydroxylation procedure began by having neighboring hydroxyls combine to form water, with subsequent water removal. This can only occur to a limited extent without necessarily creating defects, when more energy is required to remove additional hydroxyls, and thus leave strained, or defect, sites behind. In the final stages of dehydroxylation, Peri allowed for the migration of hydroxyls, oxide ions, and finally aluminum atoms to remove the last traces of water and to create a surface with the least amount of strain. Peri's use of a computer and stringent rules for the removal of hydroxyls led him to assign the five OH IR bands by assuming that the determining factor in the assignment is the number of nearest oxide neighbors at the surface. His assignments, however, do not account for OH ligands in any configurations other than octahedral, such as tetrahedrally coordinated sites, and is thus too restrictive a model for any real alumina other than an α-alumina surface. It is also unclear what the consequences of the necessary decrease in surface area of the model upon dehydroxylation and atom rearrangement may have on the final energy of the system. One can, however, imagine that there may be significant fractions of any alumina surface in which only the (100) plane is preferentially and solely exposed, and Peri's model may be helpful in characterizing these "(100) islands".

The mentioned weak points in Peri's assignment were noted by Knozinger et al.,[7] who also presented a model for alumina surfaces incorporating the (110) and the (100) faces, as well as the (111) face, for γ-alumina. Knozinger assigned the five IR bands according to the net charge of the five types of hydroxyl groups which occur on the surface of γ- and η-aluminas, with the type Ia hydroxyl being the most basic and the type III hydroxyl being the most acidic. Knozinger also used the relative basicities of the hydroxyls to describe the pathways by which the surface hydroxyls may be removed, with the most basic hydroxyls being removed first. With this model there is no way of knowing the relative amounts of each type of hydroxyl on a surface, and transition-aluminas with different surface areas more than likely will have differing proportions. The coupling of this model with IR experiments performed on a series of dehydroxylated aluminas can, however, give one insight into which planes are exposed under such conditions. It is not clear from these models what the relative amounts of surface T_d and O_h sites might be.

The NMR of catalytic surfaces has also had an impact on the current school of thought concerning those surfaces. For example, proton NMR studies of transition-aluminas by Pearson[4] revealed that there are two types of protons on the surface: those associated with physisorbed water and those with chemisorbed water. Pearson also showed that the proton line width for transition-aluminas containing no physisorbed water was inversely proportional to the BET surface area of that alumina and reasoned that this was attributable to the less mobile interior protons exchanging with the more mobile surface protons. Pearson then attempted to determine the concentration of protons within the first two molecular layers of a transition-alumina. He did this by using a model proposed by O'Reilly,[9] which suggested that the first two surface layers of an alumina did not contribute to the ^{27}Al solid-state NMR of the alumina. Pearson used this model to extrapolate his proton line width data and determined the fraction of protons which would be within two molecular layers of the surface. Using his equations, a γ-alumina with a surface area of 220 m^2/g would have 83.1% of its protons in the first two molecular layers of the surface. Other nuclei pertaining to aluminas which have been observed through solid-state NMR include ^{27}Al NMR of aluminas[5] and the ^{15}N of labeled pyridine adsorbed onto alumina surfaces.[10] These experiments have shed light on the types of aluminum environments present at the surface, i.e., O_h and T_d sites, and Lewis acid sites, respectively. These examples certainly do not exhaust the possibilities of what information can be obtained concerning the surfaces of aluminas through NMR but open doors to what can be learned.

Given the variety of methods available to describe alumina surfaces, it is not surprising that conflicts may arise in the interpretation of these data. For instance, IR results are not always

(3) Peri, J. B.; Hannan, R. B. *J. Phys. Chem.* **1960**, *64*, 1526.
(4) Pearson, R. M. *J. Catal.* **1971**, *23*, 388. Schreiber, L. B.; Vaughan, R. W. *J. Catal.* **1975**, *40*, 226–235.
(5) Morris, H. D.; Ellis, P. D. *J. Am. Chem. Soc.* **1987**, *109*, 1648.
(6) Peri, J. B. *J. Phys. Chem.* **1965**, *69* (1), 220.
(7) Knozinger, H.; Ratnasamy, P. *Catal. Rev. Sci. Eng.* **1978**, *17* (1), 31.
(8) Flank, W. H. *Clays Clay Miner.* **1979**, *27* (1), 11.
(9) O'Reilly, D. E. *Adv. Catal.* **1960**, *12*, 31.
(10) Majors, P. D.; Ellis, P. D. *J. Am. Chem. Soc.* **1987**, *109*, 1648.

supported by other methods. One such report involves some intriguing results obtained with ^{27}Al NMR. O'Reilly,[9] through a series of solid-state ^{27}Al NMR experiments on transition-aluminas, including α- and γ-alumina, concluded that there is a very large electric field gradient (efg) affecting the top two surface layers of aluminum atoms, the size of the efg being large enough to make the aluminum atoms unobservable by NMR techniques. The efg arises due to the interaction of a nucleus with the gradient of the electric field due to a distribution of point electric charges around it. A less symmetric environment about the aluminum atoms will thus create a larger efg, while a nucleus with T_d or O_h symmetry will experience no efg, and consequently will have no quadrupolar coupling constant, Q_{cc}. IR data support five types of hydroxyls on the surface, and thus five types of aluminum environments; see Figure 1. The geometries of these aluminum atoms do not suggest that they would be subject to anomolously large efg's, but instead draw a picture of the surface not unlike that of the bulk. O'Reilly's conclusions also conflict with results obtained from a cross-polarization experiment performed in this laboratory in which surface aluminum atoms were selectively detected.[5]

In all fairness to O'Reilly, it is difficult to look at most structures and predict their electric field gradient tensors. Because of this, and to attempt to gain further understanding of the NMR results, we will present the results of several ab initio MO calculations of the efg for a variety of aluminum model compounds of the type illustrated in Figure 2. It should be noted that the model clusters we describe are not unlike those used in MO calculations of surface site acidities and basicities by Kawakami and Yoshida.[11]

If there were no systematic errors in O'Reilly's experiments, and since the presence of a large efg at the surface aluminum atoms is not supported by other experimentation, then why could O'Reilly not observe all of the aluminum magnetization? One explanation could lie in the formulation of a surface with dynamic characteristics. Exchange between chemisorbed and physisorbed water via water formation, and subsequent water movement followed by dissociation from the surface, along with more discrete dynamics such as proton hopping, could set up an efficient quadrupolar relaxation pathway for the surface aluminum atoms which could also lead to extremely broad resonances.

A proposed dynamic model can be tested in the laboratory by comparing the results of low-temperature and room-temperature NMR experiments. An increase in signal is expected for all samples at lower temperatures due to the Boltzmann factor, after allowing for relaxation effects and changes in the Q of the probe. If, however, upon lowering the temperature there is a slowing of the dynamics which broaden resonances at higher temperatures, then one should observe an increase in signal *greater* than the Boltzmann factor due to the narrowing of the resonance. Relative T_1's should also indicate a slowing of the motion which facilitates relaxation at room temperature at lower temperatures. Through variable-temperature ^{27}Al NMR of transition-aluminas and dehydroxylated γ-alumina, we will demonstrate the types of exchange mechanisms mentioned above and describe their consequences on the ^{27}Al signal intensity.

Postulated models and experimentation have shown that the surfaces of aluminas are very complex. Any model proposed to describe these surfaces would require a large basis from which to formulate structures, as well as some educated speculation regarding how the large number of variables needed to describe the surface should be brought together. It is not apparent from previous work that the surface may be dynamic in nature. It is our intent to describe a surface which is dynamic and thus added to the general knowledge of aluminas, as well as dispel some previous notions concerning alumina surfaces.

Experimental Section

Sample Preparation. The α-alumina (Norton catalyst support No. SA 5551) and γ-alumina (Norton catalyst support No. SA 6173) were ob-

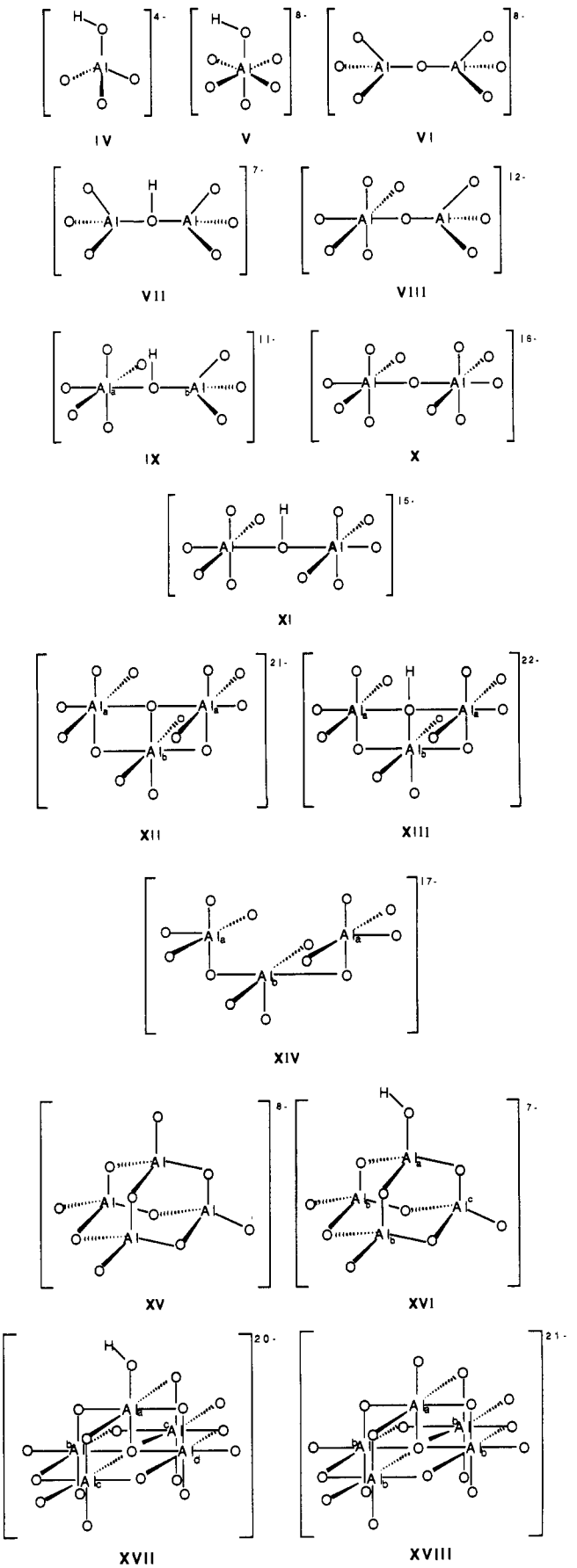

Figure 2. Some representative model surface alumina clusters which were used in the MO calculations of the aluminum efg values. Bond angles were either 90° or tetrahedral (109.471 221°). Aluminum–oxygen bond lengths were 1.81 Å, while the oxygen–hydrogen bond lengths were 1.0 Å.

(11) Kawakami, H.; Yoshida, S. *J. Chem. Soc., Faraday Trans. 2* **1985**, *81*, 1117–1137.

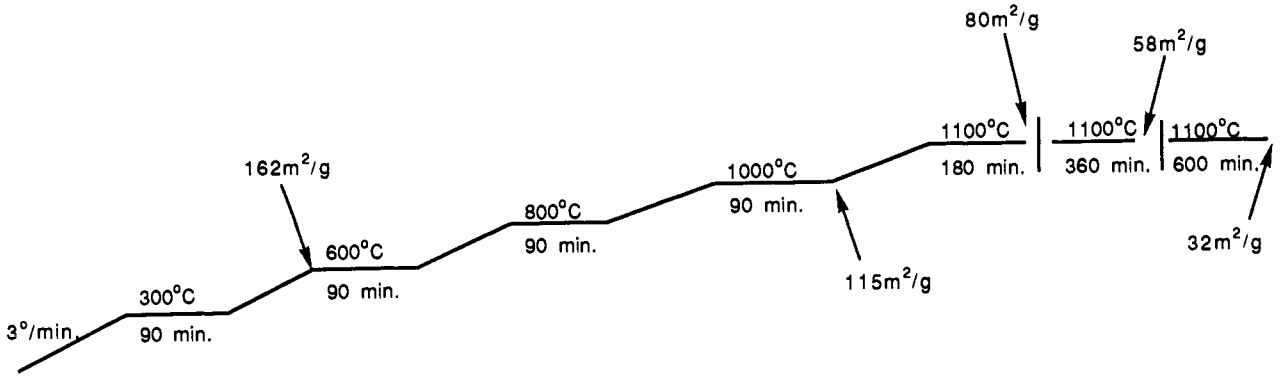

Figure 3. Ramp rates (3 °C/min) and temperatures used in the production of transition-aluminas from boehmite. The arrows indicate the time and temperature at which the sample was removed from the programmable tube furnace. All surface areas were determined by the average of three cycles on a Quantachrome surface area analyzer.

Table I. Percent by Weight of Physisorbed Water on α-, γ-, and Some Transition-Aluminas

surface area (m^2/g)	% physisorbed water	surface area (m^2/g)	% physisorbed water
220	7.2	57	1.3
160	4.1	32	0.93
115	3.6	0.25	2.4
80	5.1		

tained as gifts from Norton, Inc. These catalyst support pellets were carefully ground with a mortar and pestle to a fine white powder, placed in a capped jar, and used without any further drying; these will be described as untreated aluminas. The transition-aluminas were prepared by heating boehmite (γ-alumina monohydrate) in a programmable tube furnace at fixed times and temperatures, as shown in Figure 3. As previously mentioned, the final surface characteristics are dependent upon sample preparation. Therefore, all of the samples were treated under the same conditions until a greater temperature and/or more time was needed in order to create samples with lower surface areas. These intermediate aluminas were also stored in capped jars and used without further drying. The surface areas of these aluminas were determined by taking the average of three runs with a Quantachrome surface area analyzer, using the BET[12,13] method, giving an error of no more than ±2 m^2/g. The three dehydroxylated samples, partially dehydroxylated alumina (PDA), intermediately dehydroxylated alumina (IDA), and extremely dehydroxylated alumina (EDA), were prepared from γ-alumina according to Majors.[10] These samples were sealed under vacuum and packed into air-tight rotors (in the sense that oxygen-sensitive samples can remain in the probe for several days without noticeable sample decomposition) in a nitrogen atmosphere drybox. Upon heating, the surface areas of these samples did deviate from that of γ-alumina, 220 m^2/g, and are, for PDA, IDA, and EDA, 212, 211, and 177 m^2/g, respectively.

Because these experiments were of a quantitative nature, it was important to know the number of aluminum atoms in each sample. Therefore, the amount of physisorbed water in each sample was determined. This was accomplished by weighing an amount of material in a sample cell used with the surface area analyzer, degassing the sample on the Analyzer at 105 °C for 30 min, and reweighing the sample. The results given in Table I correspond to the average of three trials for each sample.

Spectra. All solid-state ^{27}Al NMR measurements were taken at a Larmor frequency of 104.21 MHz on a Varian XL-400 spectrometer operating in the wide-line mode. The probe used was a multinuclear 7-mm MAS probe designed and manufactured by Doty Scientific (600 Clemson Rd., Columbia, SC). Bloch decays were recorded for each of the samples with no decoupling, and the signal was referenced to that of $Al(NO_3)_3 \cdot xH_2O$. The 90° pulse widths were determined using liquid $AlNH_4(SO_4)2 \cdot 12H_2O$ and were found to be 6.0 μs, giving a 2.0-μs pulse width for the inner $\pm^1/_2$ transition. However, to obtain quantitative results,[14,15] 3° flip angles were used, resulting in a 0.2-μs pulse. The number of transients for all ^{27}Al spectra was 16. To show that we were observing all of the aluminum spins, a calibration experiment, which will be described subsequently, was performed with $Al(NO_3)_3$ in solution and α-alumina. The room-temperature studies were performed at an average of 293 ± 3 K, while the lower-temperature experiments were run at an average of 90 ± 5 K.

Results and Discussion

The characterization of surfaces, and especially alumina surfaces, has been the subject of many studies.[1-10] There have been many discoveries which have changed the way in which chemists think about surfaces, some of which have come about with the aid of solid-state NMR spectroscopy. D. E. O'Reilly[9] examined the solid-state ^{27}Al NMR of α- and γ-alumina. α-Alumina, surface area 1 m^2/g, gave an NMR signal which was almost 67% stronger than that due to γ-alumina, surface area 200 m^2/g. O'Reilly also obtained data on a series of transition-aluminas with varying surface areas at room temperature and found that, for an equal number of aluminum nuclei, each of the aluminas had a weaker signal that the α-alumina. Under normal Bloch decay conditions, one would expect the signal to arise from the whole of the sample, i.e., from the bulk and surface aluminum atoms, and thus for an equal number of spins, one would expect to obtain the same signal intensity. This is not what O'Reilly observed. He reasoned that the reduction in observed signal was because the surface aluminum atoms possessed a large electric field gradient. Such a large efg would make the resulting surface aluminum Q_{cc} sufficiently large as to render the signal broadened beyond detection by the NMR experiment. O'Reilly calculated that on average the first two molecular layers of the aluminas would be so effected and that the bulk would be unchanged by the effect, thus accounting for the increase in signal as surface area decreased.

O'Reilly's observations at first glance are hard to accept but, as will be shown, are correct. However, doubt concerning his conclusions is just and founded in previous IR data[7] as well as a surface-selective cross-polarization (CP) experiment utilized in this laboratory.[5] IR investigations suggest that the structures of surface aluminum atoms are not dramatically different from those of bulk aluminum sites; i.e., aluminum atoms at the surface are not in environments which would give rise to such large efg's; see Figure 1. In addition, the CP experiment does not support the conclusion that surface aluminum atoms are unobservable by ^{27}Al NMR. The ^{27}Al CP experiment was performed on γ-alumina using the surface OH groups as the proton source for magnetization transfer. The experiment is surface selective because the surface OH groups make up the only significant proton population in aluminas and only aluminum atoms at the surface are close enough to the protons for cross-polarization to occur. The fact that a surface signal was observed strongly suggests that O'Reilly's conclusions are incorrect. If the surface aluminum atoms were broadened by a large efg, then a surface signal would not be

(12) Sormoraj, G. A. *Principles of Surface Chemistry*; Prentice-Hall: Englewood Cliffs, NJ, 1972; pp 212-222.
(13) *Quantachrome Monorb Instrumentation Manual*; Quantachrome Corp.: Syosset, NY; Section I, pp 1-3, Section III, pp 1-3.
(14) Fenzke, D.; Freude, D.; Frohlich, T.; Haase, J. *Chem. Phys. Lett.* **1984**, *111*, 171-175.
(15) Man, P. P. *J. Magn. Reson.* **1988**, *77*, 148. Man, P. P.; Klinowski, J.; Trokiner, A.; Zanni, H.; Papon, P. *Chem. Phys. Lett.* **1988**, *151*, 143.

obtained by cross-polarization techniques either. With this in mind, there must be some other reason for the anomoly observed by O'Reilly.

Before a discussion of the results of our solid-state ^{27}Al NMR studies, it is important to establish that we are indeed observing all of the aluminum magnetization. Quantitation of ^{27}Al solid-state NMR spectra is known to be fraught with difficulties. Several workers[14,15] have presented methods in which small flip angles (5–10°) are used to excite the aluminum atoms. This experiment has demonstrated good quantitation with ^{27}Al and ^{23}Na NMR. In order to demonstrate, we were observing all of the aluminum spins in an inert and stable α-alumina; the ^{27}Al NMR of a known amount of $Al(NO_3)_3$ in solution was run at room temperature with a flip angle of 9.2°. The integral of this spectrum was compared to the integral of the room-temperature ^{27}Al spectrum of a weighed amount of α-alumina in which a 9.0° flip angle was used. The number of aluminum atoms in the α-alumina sample was calculated by using the formula Al_2O_3 and by taking into account the small percentage of physisorbed water as discussed in the Experimental Section. The integrals were normalized to the number of aluminum atoms in each sample, and then the value from the α-alumina was scaled further to account for the fact that we were observing the $\pm^1/_2$ transition and for pulse width differences between the two samples. The two normalized values in arbitrary units are 10.33 for the solid α-alumina and 10.22 for the $Al(NO_3)_3$ and agree to within experimental error, which is ±5% for this experiment. Therefore, it can be said that we are indeed observing all of the aluminum spins in the α-alumina sample. The α-alumina, then, is our standard to which all other alumina spectra will be referenced.

As we are able to successfully quantitate our aluminum signal, our notion of a dynamically broadened line shape can be tested by utilizing low-temperature NMR experiments. A line shape which is inhomogeneous in nature, such as that created by a static sample, i.e., one with no associated dynamics, is comprised of overlapping narrow isochromats which span the entire spectrum. This inhomogeneous line shape is not temperature dependent in the sense that it will not narrow upon lowering the temperature but will only show an increase in signal intensity governed by the Boltzmann factor and temperature-dependent probe factors. A dynamically broadened line shape is homogeneous and thus behaves as a single broad line shape. This line shape will narrow if the temperature is dropped sufficiently to slow the dynamics responsible for the broadening at higher temperatures. Therefore, if thermally activated surface dynamics are the reason for the undetectably broad ^{27}Al resonance, then as the temperature is lowered, the motion causing the extreme broadening will be slowed and the signal for all aluminas will become equal in the limit of no motion.

The ^{27}Al solid-state NMR was therefore performed on α- and γ-aluminas and on a series of transition-aluminas at room temperature and at approximately 90 K. In accordance with O'Reilly's results, the γ-alumina (220 m^2/g) gave a normalized ^{27}Al signal of only 55% of that for the α-alumina at room temperature under our experimental conditions. The static ^{27}Al Bloch decay spectra of α-, γ-, and transition-aluminas (80 m^2/g) at 290 and 90 K are shown in Figure 4. The broad resonance at ~0.0 ppm is due to the octahedrally coordinated, O_h, aluminum atoms, while the tetrahedrally coordinated, T_d, aluminum atoms are responsible for the shoulder at ~65 ppm. The signals in these spectra are due to bulk and surface aluminum atoms. A plot of surface area vs calculated and experimental intensity gain at 290 ± 3 and 90 ± 5 K for the entire series studied using Bloch decays (in the presence of strong ^1H decoupling) is shown in Figure 5. The experimental signal intensities were calculated by multiplying the integrated signal by $1/g_{sample}$, where g_{sample} is the mass of the alumina sample, taking into account the percent of physisorbed water. It is clear from this plot that the higher surface area aluminas are experiencing a greater than calculated gain as compared to α-alumina. The variation in calculated gain for each alumina sample reflects small differences in the temperatures at which the spectra were taken. As is also evident, the α-alumina's

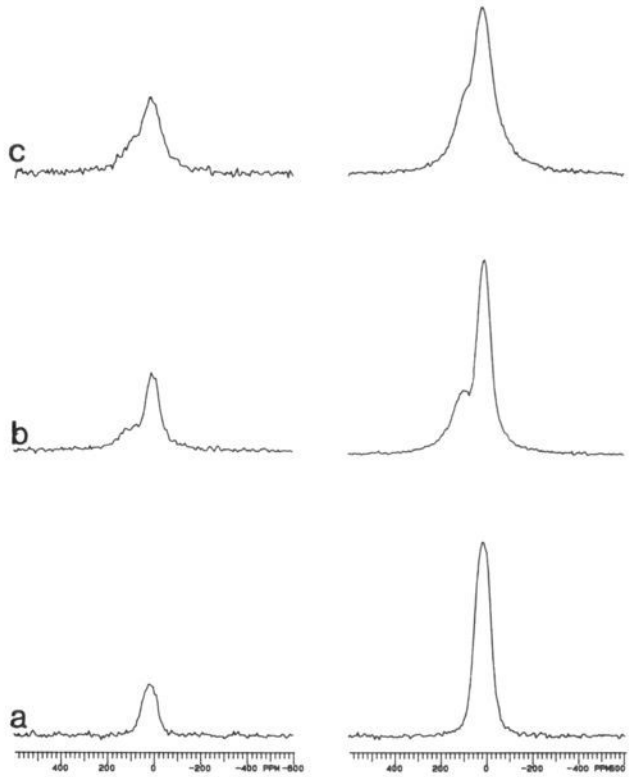

Figure 4. Static ^{27}Al NMR spectra of (a) α-alumina, (b) an 80 m^2/g transition-alumina, and (c) γ-alumina at 290 K, left column, and at 90 K, right column. Each is an accumulation of 16 transients. The spectra are not on the same scale.

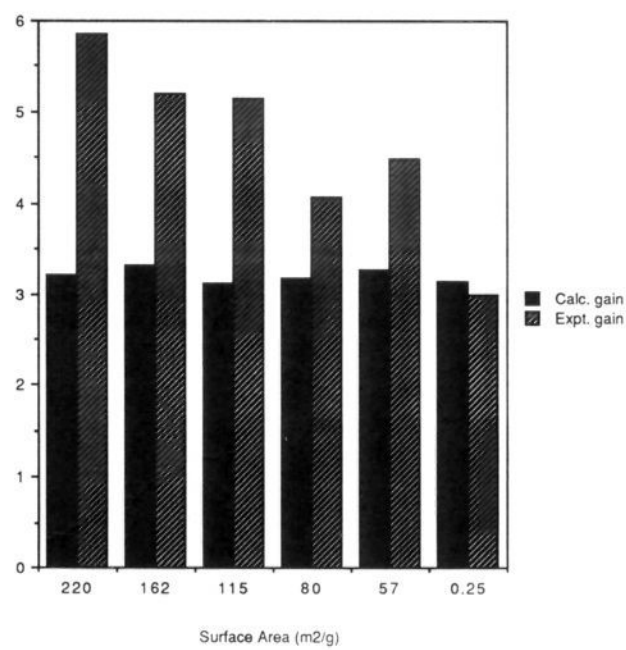

Figure 5. Plot of the alumina surface area vs the experimental gain in signal and calculated gain in signal from 90 to 290 K. The experimental gain was calculated simply by dividing the low-temperature signal by the high-temperature signal. The calculated gain was determined by dividing the high temperature by the low temperature used experimentally. The change in probe Q over this temperature range was less than 1%.

calculated gain is greater than its experimental gain. This reflects overall errors in the experiment, as well as the longer T_1 of α-alumina at 90 K. A delay of 30 min was used for the α-alumina at 90 K, which may not have been long enough for complete relaxation. The largest error in the data for each sample comes

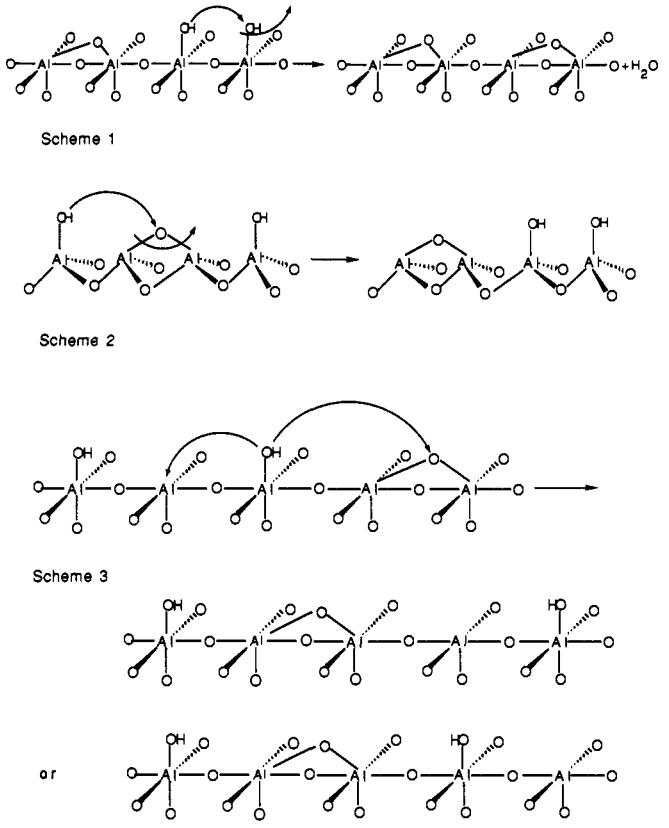

Figure 6. Proposed mechanisms for water motion on alumina surfaces. See text for explanation of schemes.

from the actual integration of the spectra. This is because the samples do not have the same type of line shape nor do they have the same line widths, a matter which will be discussed below. These factors, as well as integration being a subjective technique, give rise to a conservative estimate of the error as ±10%.

It is clear from the results shown in Figure 5 that we are indeed regaining some of the "lost" signal at low temperatures, as the gain in signal is greater than the calculated Boltzmann and probe Q factors, or calculated gain. This intriguing phenomenon may be explained by a model of a surface which is dynamic, which could also result in a ^{27}Al line shape which is broadened beyond detection. Why, then, is all of the signal not regained at 90 K? One answer may be that even at 90 K all of the surface dynamics are not stopped. The types of dynamics which could be occurring on an untreated alumina surface are shown in Figure 6. This figure is not intended to describe the surface of any particular alumina, but only to illustrate the mechanisms of motion which could be occurring on a given surface. Scheme 1 depicts the formation of water by the combination of two neighboring hydroxyls, leaving behind a bridging oxygen. In this scheme, the water formed is free to tumble across the surface, leave the surface, or reassociate. A reassociation of the water could either form two adjoining hydroxyl groups or cap a Lewis acid site. This type of mechanism would be expected to occur to a great extent on untreated aluminas because of the large population of surface hydroxyls. Scheme 2 depicts a more discrete movement of surface protons. This type of motion has the affect of rearranging hydroxyl positions and can occur on an alumina surface where the physisorbed water has or has not been removed. The migration of a Lewis acid site is shown in Scheme 3. This mechanism also amounts to the movement of a hydroxyl group. Again, this scheme could occur on an alumina surface with or without physisorbed water, although the presence of Lewis acid sites would be expected to increase as the concentration of physisorbed water decreased. The decrease in signal with increase in surface area can thus be explained in part by these types of dynamics creating an efficient quadrupolar relaxation pathway for the surface aluminum atoms at room temperature. It is reasonable that a dynamic process including water (Scheme 1) would be significantly slowed or even stopped at 90 K, but a proton hopping motion (Schemes 2 and 3) might only be slightly slowed. This proton hopping would continue to affect the NMR line shape at 90 K but may not have as large of an affect on the quadrupolar relaxation by itself, especially on an untreated alumina which contains a large amount of physisorbed water. In other words, the greater amount of surface hydroxyls on an untreated alumina could dampen the dynamics of Schemes 2 and 3. This is why there is less than 100% gain in signal at 90 K for the transition-aluminas when compared to α-alumina. Therefore, O'Reilly was correct in that the surface aluminum atoms are perturbed, not by a large electric field gradient as he proposed, but rather by motion at the surface. Such a motion might affect not only aluminum atoms at the surface but could also have a trickle-down affect through the first two or three molecular layers of the alumina, as the electronic environments of the surface oxygens and aluminum atoms are perturbed and carry this effect down to subsurface sites.

As previously mentioned, there have been many experimental techniques used to describe alumina surfaces, some of which are difficult to perform because of the nature of the surface. IR measurements fit into this category. One method which might be utilized to support the IR information, as well as our NMR results, is to use the five aluminum models predicted by IR, as well as some other models, in the ab initio calculations of electric field gradients of the aluminum atoms. Initially, the models can be run separately as a basis for a simple surface; then, the different groups may be combined to form a framework for a more realistic system. The calculated efg's will allow the determination of the corresponding Q_{cc}'s, subject to the limitations imposed by Sternheimer antishielding effects,[16] and thus a comparison to those values calculated from the analysis of the ^{27}Al NMR line shapes will be possible. Another way in which calculated efg's may be used is in the formulation of an exchange process. Different surface sites undergoing exchange could also help to explain the loss in signal intensity with increased surface area. An aluminum atom with a Q_{cc} on the order of 4–6 MHz exchanging with an aluminum atom with a Q_{cc} of 25 MHz would give rise to the narrower resonance being broadened, the extent of which would depend upon the rate of exchange, as will be discussed. By exchanging, it is not meant that the aluminum atoms are actually moving but that their environment is changing via proton motion, giving rise to varying Q_{cc}'s. Thus, the calculated efg's, and therefore Q_{cc}'s, will help to determine if this process may be used to describe the surface.

Electric Field Gradient Calculations. The nuclear quadrupole coupling constant is parametrically dependent upon the zz component of the electric field gradient tensor, q_{zz}, i.e., (e^2Qq_{zz}/h). The other symbols, e, Q, and h are the charge of the electron, the quadrupole moment of the nucleus of interest, and Planck's constant, respectively. The zz element of the field gradient tensor can be expressed as[17]

$$q_{zz}^{1} = \sum_{K} Z_K \frac{[2Z_{1K}Z_{1K} - (X_{1K}^2 + Y_{1K}^2)]}{R_{1K}^5} - \sum_{k}\sum_{l} P_{kl} \left\langle \chi_k \left| \frac{2z_1z_1 - (x_1^2 + y_1^2)}{r_1^5} \right| \chi_l \right\rangle \quad (1)$$

The first summation extends over the number of atoms, whereas the double summation is over the number of basis functions. Further, the uppercase symbols X_{1K}, Y_{1K}, and Z_{1K} refer to the nuclear coordinates associated with the vector from nucleus I to K. The lower case symbols x_1, y_1, and z_1 refer to the components of the vector from the nucleus I to the electron. Z_K denotes the nuclear charge on atom K. The symbols P_{kl}, χ_k, and χ_l refer to the kl element of the density matrix and basis functions k and

(16) Cohen, M. H.; Reif, F. *Solid State Phys.* **1957**, *5*, 347. The Sternheimer effects should be negligible in our calculations due to the ab initio formulation of the problem.

(17) Kern, C. W.; Karplus, M. *J. Chem. Phys.* **1965**, *42*, 1062–1071.

Table II. Basis Set Dependence of the q_{zz} for $[O_3AlOH]^{3-}$ [a]

basis set (nbf)[b]	q_{zz} (au)	η	energy (au)	time (cpu)[c]
STO-3G (30)	−0.903 755	0.01	−532.525 431 584	1.0
STO-6G (30)	−0.976 896	0.01	−537.358 833 313	3.78
3-21G (51)	−0.309 110	0.01	−537.722 247 997	3.06
3-21G* (57)	−0.333 480	0.02	−537.807 483 639	4.66
6-31G (51)	−0.267 989	0.04	−540.735 783 740	4.20
6-31G* (81)	−0.300 058	0.01	−540.795 761 355	26.50
6-31G** (84)	−0.297 768	0.01	−540.801 965 065	29.32
D-95 (60)[d]	−0.318 956	0.01	−540.874 071 742	10.61
6-311G** (104)	−0.274 156	0.05	−540.957 237 701	55.21

[a] The geometry employed in these calculations is as follows: the Al–O bond distance was 1.81 Å, the O–H bond distance was 1.00 Å, and the bond angles were tetrahedral, i.e., 109.471 221°. [b] An excellent discussion of definition of the various basis sets is described in: *Ab Initio Molecular Orbital Theory*; Hehre, W. J., Random, L., Schleyer, P. v. R., Pople, J. A., Eds.; Wiley: New York, 1986; Chapter 4, pp 65–91. The number in parentheses is the number of basis functions for the molecule of interest. [c] Times are relative to the cpu times obtained on a VAXStation 3540; e.g., the cpu time for the STO-3G calculation was 188 s. [d] Dunning, T. H.; Hay, P. J. *Modern Theoretical Chemistry*; Plenum: New York, 1976; Chapter 1, pp 1–28.

l, respectively. The symbols R_{1K} and r_1 refer to the scalar internuclear distance between nuclei I and K and the distance to the electron and nucleus I, respectively.

From the form of the gradient operator, it is clear that for systems of O_h symmetry q_{zz} will be zero. This is due to the isotropy of the space; i.e., the integrals over $x_1x_1(r_1^{-5})$, $y_1y_1(r_1^{-5})$, or $z_1z_1(r_1^{-5})$ will be equal. Likewise, the geometrical factors in the first term of eq 1 will zero for the same reasons. However, for the discussion here it is the distortion from O_h and T_d symmetry that is of interest.

The field gradient is expressed in atomic units. These units can be converted to Q_{cc} (in megahertz) values for aluminum by the following equation:

$$Q_{cc} = q_{zz}(e^2Q_{Al}/a_0^3h) = q_{zz} \times 35.00977 \text{ MHz} \quad (2)$$

Before one can accurately calculate q_{zz}, one must explore the basis set dependence of the calculated values of q_{zz} for a simple molecule. For the systems of interest here, we have chosen the tetrahedral surface fragment $[O_3AlOH]^{3-}$. The various basis sets were selected from the GAUSSIAN 90 program.[18] The results of such a series of calculations are summarized in Table II. It is clear that, except for the smallest basis sets (STO-3G and STO-6G), the predicted value of Q_{cc} ranges from −11.68 to −9.38 MHz; i.e., q_{zz} ranges from −0.333 480 to −0.267 989 au. As a reasonable compromise between cpu time and the quality of the calculation, as reflected in the computed energy, we have selected the D95 basis set to use in subsequent calculations.

The model systems employed in our field gradient calculations are summarized in Figure 2. These structures are meant to model the five different types of structures proposed from the IR data, i.e., structures I–III depicted in Figure 1. Proposed sites IA and IB (see Figure 1) are modeled by structures IV and V, respectively, of Figure 2. Sites IIA and IIB (see Figure 1) are modeled by structures VI–XI, respectively, of Figure 2. Structures VI and VII of Figure 2 were included for completeness. Proposed structure III (see Figure 1) is modeled by structures XII and XIII of Figure 2. Further, in an attempt to model Lewis acid sites, we have performed calculations on structure XIV of Figure 2. Additionally, to complete our modeling of Brønsted sites on the surface, we have also performed calculations on the clusters depicted is structures XV–XVIII of Figure 2. All of the structures employed for these calculations are idealized in the sense that no attempt was made to optimize the geometry of any given structure. Such optimizations appear to us to be premature at this point.

(18) GAUSSIAN 90, Revision F: M. J. Frish, M. Head-Gordon, G. W. Trucks, J. B. Foresman, H. B. Schlegel, K. Raghavachari, M. Robb, J. S. Brinkley, C. Gonzalez, D. J. Defrees, D. J. Fox, R. A. Whiteside, R. Seeger, C. F. Melius, J. Baker, R. L. Martin, L. R. Kahn, J. J. P. Stewart, S. Topiol, J. A. Pople, Gaussian, Inc., Pittsburgh, PA, 1990.

Table III. Predicted[a] Electric Field Gradients, Quadrupole Coupling Constants, Asymmetry Parameter, Charge Density, and Energy for Potential Surface Models for Aluminum Oxide

structure	q_{zz} (au)	Q_{cc} (MHz)	η	charge	energy (au)
		T_d Sites			
IV	−0.318 956	−11.17	0.01	1.443	−540.874 071 742
VI	0.129 169	4.522	0.16	1.337	−1003.669 248 68
VII	−0.343 264	−12.02	0.66	1.318	−1005.308 637 08
VIIIb	0.238 012	8.333	0.00	1.170	−1147.560 061 72
IXb	0.110 245	3.860	0.38	1.480	−1149.923 813 03
XV	0.029 960	1.049	0.00	1.629	−1713.460 561 57
XVIa	−0.306 498	−10.73	0.00	1.697	−1714.925 122 22
XVIb	−0.110 306	−3.862	0.61	1.639	
XVIc	−0.104 467	−3.657	0.66	1.641	
		O_h Sites			
V	−0.191 839	−6.716	0.20	1.380	−686.170 562 623
VIIIa	−0.156 076	−5.464	0.00	1.520	
IXa	−0.263 415	−9.222	0.18	1.499	
X	0.085 917	3.008	0.00	1.088	−1289.047 922 34
XI	−0.072 056	−2.523	0.37	1.385	−1292.152 850 67
XIIa	−0.077 307	−2.706	0.21	0.772	−1749.238 330 28
XIIb	0.085 131	2.980	0.05	0.956	
XIIIa	−0.196 781	−6.889	0.51	0.905	−1752.574 945 44
XIIIb	−0.370 829	−12.98	0.43	1.194	
XIVa	−0.699 196	−24.48	0.14	1.162	−1679.600 861 31
XIVb	−0.732 584	−25.65	0.26	1.096	
XVIIa	−0.390 285	−13.66	0.18	0.916	−2532.779 820 58
XVIIb	−0.260 327	−9.114	0.52	0.841	
XVIIc	−0.287 728	−10.07	0.15	0.779	
XVIId	−0.288 073	−10.08	0.27	0.752	
XVIIIa	−0.270 202	−9.460	0.00	0.804	−2529.639 372 67
XVIIIb	−0.302 424	−10.59	0.07	0.740	

[a] All calculations were performed using the D95 (see Table I, ref d) basis set from GAUSSIAN 90.

Table IV. Experimental Line Widths at Half-Height (lwhh) for ^{27}Al Bloch Decay and Cross-Polarization Signals of Aluminas

surface area (m^2/g)	lwhh (kHz) at 290 K	lwhh (kHz) at 90 K
	Bloch Decay	
220	12.48	13.30
162	13.10	11.47
115	9.49	10.24
80	7.52	7.72
58	7.30	7.63
1	7.82	8.20
212[a]	16.33	14.61
211[b]	11.41	15.49
173[c]	14.15	13.80
	Cross-Polarization	
220	6.74	7.61
162	7.75	
115	6.64	
80	8.18	
32	7.57	
212[a]	5.32	

[a] PDA. [b] IDA. [c] EDA.

Our aim here is to identify structure types that may be important at the surface rather than to produce a detailed proposal, including bond distances and angles, for what the structure of the surface may be. Hence, we have employed the structural parameters summarized in the caption for Figure 2.

The results of our calculations are summarized in Table III. In addition to the values of q_{zz}, Q_{cc}, η, and energy, we have included a summary of the charge at the aluminum atom as well. The first point that is apparent from Table III is that the quadrupole coupling constant for the aluminum changes its sign from one coordination geometry to another. Further, the T_d sites can be of either sign (−11.17 to +8.33 MHz), whereas the O_h sites are generally negative except when they are small, when they can have both signs, i.e., −25.65 to +3.01 MHz. The second point that can be made is that the magnitude of the predicted coupling constant,

with the exception of the Lewis acid site structure, XIV, is typically less than 12 MHz. As we shall show subsequently, the value observed for the Q_{cc} of surface T_d and O_h sites is on the order of 5–6 MHz. Hence, it appears that the calculation may be overestimating the value of Q_{cc} by a factor of 2, again subject to Sternheimer antishielding effects,[16] or that this difference reflects the quality of the model structures used to simulate the surface. In any event, the only structures which appear to have large field gradients are those associated with the Lewis acid sites. It is also apparent from Table III that the net charge on the aluminum atom is not easily correlated with the calculated value of Q_{cc}; i.e., compare IV and VI for T_d sites and X for XIVb for O_h sites. However, before proceeding, we will consider the sensitivity of the predicted Q_{cc} values to model geometry and to the presence or absence of a H at a terminal or bridging O atom.

For the T_d sites we can compare structures IV and XVI in Figure 2. The quadrupole coupling constant only changes from −11.17 MHz (IV) to −10.73 MHz (XVIa). Hence, the Q_{cc} for T_d sites does not appear to be a strong function of cluster size, at least as reflected in these calculations. The sensitivity of Q_{cc} for O_h sites can be seen from a comparison of the results for structures V and XVIIa. These results are −6.72 and −13.66 MHz, respectively. Hence, the O_h sites are more sensitive than the T_d sites to the size of the cluster used for the simulation. The calculations predict that for both T_d and O_h sites the Q_{cc} for the aluminum will be sensitive to the presence or absence of a H atom at either bridging or terminal oxygen atoms, i.e., XV vs XVIa, VI vs VII, XII vs XIII, XVIIIa vs XVIIa, and VIII vs IX. These results strongly suggest that motion of the H atoms could serve as an efficient means of modulating the Q_{cc} for a given site.

From the results of these calculations one would predict that if the surface aluminum atoms were capped by either OH groups or bridging O atoms, the resulting Q_{cc} values would only differ by about a factor of 2. Such a situation could not explain the observed losses in signal from the aluminum atoms at the surface. Hence, one must consider other types of surface sites. One such site could be a Lewis acid site, i.e., XIV of Figure 2. The value of $|Q_{cc}|$ for such a site is approximately 25 MHz. If the mean value for $|Q_{cc}|$ is approximately 7 MHz (average for T_d sites is 6.6 MHz and the average for O_h sites is 7.7 MHz) and if some dynamic process could convert this "average" surface site to a Lewis acid site, the resulting change in Q_{cc} for the "average" surface site would represent an increase by a factor of about 3.5. This increase in Q_{cc} would correspond to an increase of the width of the powder pattern by approximately a factor of 12. Hence, dynamical processes connecting Lewis acid sites could cause a significant loss in signal if the process occurred at the correct rate, that is, in the intermediate-exchange regime.

Exchange Dynamics and Powder Line Shapes. The question of the appearance of the NMR line shape for exchanging noncoupled spin systems is more complicated when the systems are in the solid state as compared to the liquid state. For the two-site problem in the liquid state, one only has to address the chemical shift difference and rate of exchange between the two resonances. The resulting line shape is sensitive to the rate of exchange relative to the chemical shift difference. The rate of exchange can be considered slow, comparable, or fast relative to the chemical shift difference, leading to the three well-known line shapes. In the case where the rate of exchange is comparable to the chemical shift difference, one finds significant losses in signal intensity. This loss is due to the signal being spread over the entire region between the two sites. When both sites are equally populated, the resulting loss is a maximum. It is this loss which is suggestive of what is happening on the surface of an alumina with regard to the ^{27}Al signal.

The characterization of the rate constants being faster, comparable, or slower relative to a chemical shift is more problematic for solid powder line shapes. This difficulty is easily visualized for a chemical exchange between two species which have the shielding powder patterns depicted in Figure 7. Here, the two $\eta = 0$ tensors differ only in their relative orientation with respect to one another, and one is the negative of the other, i.e., inversion

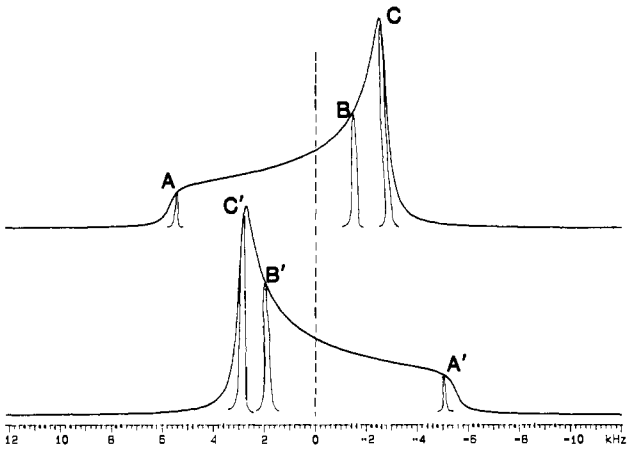

Figure 7. Representation of two $\eta = 0$ overlapping tensors. Exchange between A and A′, B and B′, and C and C′ would be slow, intermediate, and fast, respectively, if the rate of exchange was intermediate relative to the shift difference between C and the isotropic shift (denoted by the dotted line).

about the magic angle (a sign flip in the tensor parameter δ). In the top spectrum of Figure 7, we have labeled three regions which contribute to the observed line shape. In a two-site chemical exchange problem, A would exchange with A′, B with B′, and C with C′. If the rate of exchange was intermediate with respect to the "shift difference" between the isotropic shift (noted by the dotted line) and C, then the exchange rate could be considered slow relative to A and fast relative to B. Hence, the observed powder line shape for this system would have severe distortions compared to the static spectrum. Further, these distortions could be exacerbated by a spin-echo experiment. That is, further line shape distortions can result when the rate of exchange is comparable to the τ value utilized in the echo experiment. With these ideas in mind, we present the theory and some simulations as to how a powder line shape can be made to "disappear" in the presence of dynamics. The theory will be illustrated by treating the case of shielding and second-order quadrupole powder line shapes. The calculation will proceed in two parts: The first part will deal with the generation of the site frequencies needed for the exchange matrix. In the second portion we will utilize these expressions in the equations describing the time domain signal in the form of a spin-echo.

Site Frequencies.[19] The shielding case will be treated first. Further, we will limit our discussion to the two-site case. The secular portion of the anisotropic shielding Hamiltonian is given by[20]

$$H = \gamma_1 T_{20} R_{20} \tag{3}$$

where

$$T_{20} = (2/3)^{1/2} I_0 B_0 \tag{4}$$

and R_{20} contains the spatial dependence of the operator. We will rewrite the Hamiltonian for the two-site problem as

$$\mathbf{h} = \mathbf{h}_A + \mathbf{h}_B \tag{5}$$

Then, we will expand the spatial portion of $\mathbf{h}_A$ and $\mathbf{h}_B$ into the PAS frame for site A. Finally, we will expand site B into its PAS frame relative to the A frame. For our expansions we will employ the Rose conventions.[21] Hence, we can write

$$R_{20} = \sum_n D_{0n}^{(2)}(0,\theta,\phi)^* = \sum_n D_{n0}^{(2)}(-\phi,-\theta,0) \tag{6}$$

(19) Chu, P. J.; Gerstein, B. C. *J. Chem. Phys.* **1989**, *90*, 3713–3727. In this paper Chu and Gerstein develop a symmetry jump calculation for the dynamic line shape for odd multiple of a half-quadrupolar nuclides.

(20) Haeberlen, U. *High Resolution NMR in Solids: Selective Averaging*; Academic Press: New York, 1976.

where the Euler angles θ and ϕ relate the molecule fixed frame to the laboratory frame. The resulting expression for R_{20} becomes

$$R_{20} = \tfrac{1}{2}(3\cos^2\theta - 1)r_{20} + \tfrac{1}{2}(3/2)^{1/2}\sin(2\theta)[-\exp(i\phi)r_{2-1} + \exp(-i\phi)r_{21}] + \tfrac{1}{2}(3/2)^{1/2}\sin^2\theta[\exp(2i\phi)r_{2-2} + \exp(-2i\phi)r_{22}] \quad (7)$$

For site A the expansion corresponds to its PAS frame and the r_{ij}'s are given by

$$r_{20} = \rho_{20} = (3/2)^{1/2}\delta_A \quad (8)$$

$$\delta_A = \tfrac{2}{3}\Delta\sigma_A \quad (9)$$

$$r_{2\pm1} = 0$$

$$r_{2\pm2} = \rho_{2\pm2} = \tfrac{1}{2}\delta_A\eta_A \quad (10)$$

Using these expressions, one can show the site frequency for site A is given by

$$\omega_A = \omega_0[\sigma_{iso,A} + \delta_A[\tfrac{1}{2}(3\cos^2\theta - 1) + \tfrac{1}{2}\eta\sin^2\theta\cos 2\phi)]] \quad (11)$$

Here, $\sigma_{iso,A}$ denotes the isotropic chemical shift of site A. The site frequencies for site B are generated by an analogous procedure; i.e., expression 6 is substituted into each of the corresponding r_{ij}'s in eq 7. The resulting equation is then simplified by relations 8–10. After some work, the following equation can be derived

$$\omega_B = \omega_0(\sigma_{iso,B} + \mathbf{a}\sin^2\theta - \mathbf{b}\sin(2\theta) + \mathbf{c}(3\cos^2\theta - 1)) \quad (12)$$

where

$$\mathbf{a} = \tfrac{1}{4}\delta_B[c_1\cos(2\phi) - c_2\sin(2\phi)] \quad (13)$$

$$\mathbf{b} = \tfrac{1}{4}\delta_B[c_3\cos\phi - c_4\sin\phi] \quad (14)$$

$$\mathbf{c} = \tfrac{1}{4}\delta_B c_5 \quad (15)$$

$$c_1 = 3\sin^2\beta\cos(2\alpha) + \eta_B[(1 + \cos^2\beta)\cos(2\alpha)\cos(2\gamma) - 2\cos\beta\sin(2\alpha)\sin(2\gamma)] \quad (16)$$

$$c_2 = 3\sin^2\beta\sin(2\alpha) + \eta_B[(1 + \cos^2\beta)\sin(2\alpha)\cos(2\gamma) + 2\cos\beta\cos(2\alpha)\sin(2\gamma)] \quad (17)$$

$$c_3 = 3\sin^2\beta\cos\alpha - \eta_B[\sin(2\beta)\cos(2\gamma)\cos\alpha - 2\sin\beta\sin(2\gamma)\sin\alpha] \quad (18)$$

$$c_4 = 3\sin(2\beta)\sin\alpha - \eta_B[\sin(2\beta)\cos(2\gamma)\sin\alpha + 2\sin\beta\sin(2\gamma)\cos\alpha] \quad (19)$$

$$c_5 = 3\cos^2\beta - 1 + \eta_B\sin^2\beta\cos(2\gamma) \quad (20)$$

These equations where first derived by Greenfield et al.[22] and are completely general. Equations 13–20 show how two second-rank tensors can be related to one another. Here, we have related a shielding tensor to another shielding tensor. Before proceeding to the calculation of the FID, let us focus our attention on the site frequencies for the second-order quadrupole case. Following Maricq,[23] Samoson, Kundla, and Lippmaa[24] derived the following expression (corrected by Man et al.[25]) for the quadrupole Hamiltonian.

$$h_Q^{(1)} = (eQ/4I(2I-1)\hbar)^2(1/\omega_0)[2V_{21}V_{2-1}(4I(I+1) - 8I - 1)I_z + 2V_{22}V_{2-2}(2I(I+1) - 2I_z - 1)I_z] \quad (21)$$

Here, e, Q, I, $\hbar$, and ω_0 denote, respectively, the electron charge, the quadrupole moment, the value of the nuclear spin, Planck's constant divided by 2π, and the nuclear Larmor frequency. The V_{ij}'s denote the spatial portion of the field gradient tensor, and I_z is the z component of the angular momentum operator. Because of the complexity of the Hamiltonian, we will restrict our discussion to exchange sites A and B which share a common PAS frame. The extension to quadrupoles with arbitrary orientations is straightforward, but arduous, and does not add to the present discussion. The first step in the calculation is the expression of the components of the electric field gradient tensor in the laboratory frame relative to the PAS frame of site A. Using the methods outlined above, one can show

$$V_{21}V_{2-1} = \tfrac{1}{8}\delta_A^2\sin^2\theta[-\tfrac{9}{2} + 3\eta_A\cos(2\phi) - \tfrac{1}{2}\eta_A^2\cos^2(2\phi)] - \tfrac{1}{4}\eta_A^2\delta_A^2\sin^2\theta\sin^2(2\phi) \quad (22)$$

$$V_{22}V_{2-2} = \tfrac{9}{16}\delta_A^2\sin^4\theta + \tfrac{1}{8}\delta_A^2\eta_A(1 + \cos^2\theta)\cos(2\phi)[2\sin^2\theta + \tfrac{1}{2}\eta_A(1 + \cos^2\theta)\cos(2\phi)] + \tfrac{1}{4}\eta_A^2\delta_A^2\cos^2\theta\sin^2(2\phi) \quad (23)$$

Similar expressions can be generated for site B. One can now calculate the site frequencies using the following equations

$$\omega_{m,m-1} = \langle m|h_Q^{(1)}|m\rangle - \langle m-1|h_Q^{(1)}|m-1\rangle = (\omega_Q^2/\omega_0)[sV_{21}v_{2-1} + tV_{22}V_{2-2}] \quad (24)$$

where

$$\omega_Q = (e^2qQ/\hbar) \quad (25)$$

$$s = 2[4I(I+1) - 24m(m-1) - 9]/[4I(2I-1)]^2 \quad (26)$$

$$t = 2[2I(I+1) - 6m(m-1) - 3]/[4I(2I-1)]^2 \quad (27)$$

and q is the zz component of the electric field gradient tensor.

It is worth contrasting the expressions for the two cases. First, in the shielding case, chemical exchange between sites with different signs of parameter δ are important. That is, when δ changes sign, the sign of the anisotropy of the shielding tensor changes as well. Such a change could occur simply by the dissociation of an axial ligand, e.g., Cd^{2+}-substituted porphyrins.[26] This is, however, *not* the case for second-order quadrupoles. From eqs 22 and 23 it easy to see the site frequencies depend upon δ^2. Hence, an exchange process which results simply in a flip of the sign of δ will not alter the line shape. Second, the resulting exchange line shape depends linearly on the ratio of the two shielding anisotropies for the two sites. This is contrasted with the quadratic dependence exhibited for the second-order quadrupole case. Hence, small changes in the quadrupole coupling constant can have significant effects on the resulting exchange line shape. Finally, the field dependence of the two cases is of interest. In the shielding example, going to higher field corresponds to slowing the kinetic process; i.e., the interaction the dynamic process is averaging becomes larger at higher fields. In the quadrupole case, as one goes to higher field, the second-order quadrupolar interaction becomes smaller and would thus appear easier to average by the dynamic process.

Spin-Echos. In a straightforward fashion, an expression can be derived for the transverse magnetization following a two-pulse echo sequence, i.e., 90–τ–180–acq. After Greenfield et al.[22] we can write

$$g(t,\tau) = 1\exp[\mathbf{A}t]\exp[\mathbf{A}\tau]\exp[\mathbf{A}^*\tau]\,\mathbf{W}(0) \quad (28)$$

where τ is the spacing in the spin echo sequence and the remaining symbols have been previously defined. The complex conjugate of the A matrix, $\mathbf{A}^*$, is a direct consequence of the 180° pulse. The predicted spectra reported in this paper have been generated via a Fortran program which generates the spin-echo as per eq 28.

We can illustrate some of the points raised in the previous section via a simulation of the second-order line shape for the $\pm^1/_2$ transition of ^{27}Al, $I = {}^5/_2$, at 104.23 MHz (9.4T). Figure 8 gives the simulated line shapes when the value of τ is fixed at 50 μs

(21) Rose, M. E. *Elementary Theory of Angular Momentum*; Wiley: New York, 1957.
(22) Greenfield, M. S.; Ronemus, A. D.; Vold, R. L.; Vold, R. R.; Ellis, P. D.; Raidy, T. E. *J. Magn. Reson.* **1987**, *72*, 89–107.
(23) Maricq, M. M. The Effects of Sample Rotation on the NMR Spectra of Solids. Ph.D. Dissertation, M.I.T., 1979.
(24) Lippmaa, E.; Samoson, A.; Kundla, E. *J. Magn. Reson.* **1982**, *49*, 350–357.
(25) Man, P. P.; Thereneau, H.; Papou, P. *J. Magn. Reson.* **1985**, *64*, 271–277.
(26) Kennedy, M. A.; Ellis, P. D. *J. Am. Chem. Soc.* **1989**, *111*, 3195.
(27) Cheng, J. T.; Edwards, J. C.; Ellis, P. D. *J. Phys. Chem.* **1990**, *94*, 553–561.

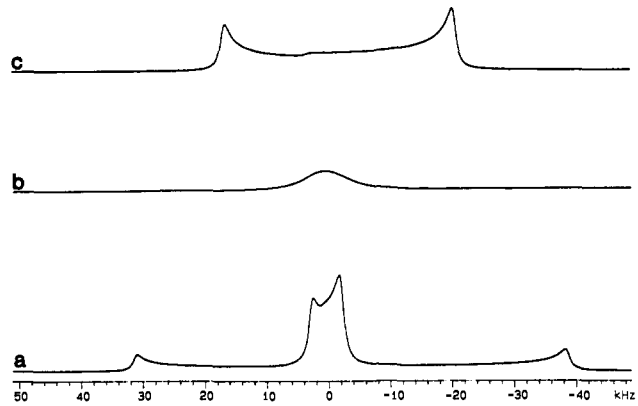

Figure 8. The simulated spectra of two overlapping tensors with Q_{cc}'s of 4 and 15 MHz undergoing exchange. These spectra were simulated using a spin-echo sequence with a τ value of 50 μs. The rates of exchange are (a) 5×10^1, (b) 5×10^4, and (c) 5×10^8, indicating slow, intermediate, and fast exchange, respectively. The spectra are plotted on an absolute intensity scale and reveal intensity loss for the intermediate exchange case.

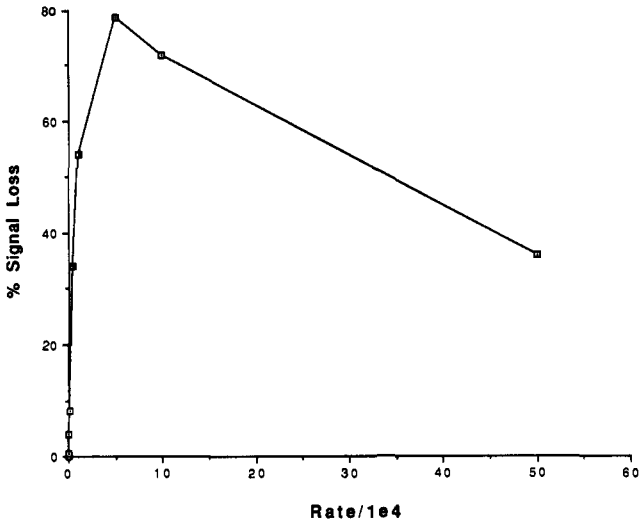

Figure 9. Plot of the percent signal intensity which is lost when two tensors with Q_{cc} values of 4 and 15 MHz are undergoing exchange with the rates given. This is calculated for a spin-echo sequence in which the τ value was 50 μs. The greatest loss is for an exchange rate of 5×10^4.

and the rate constant (k) is varied as follows: (a) 50 Hz, (b) 5×10^4 Hz, and (c) 5×10^8 Hz. The spectra represent exchange between two tensors with respective Q_{cc}'s of 4 and 15 MHz and a chemical shift difference of 50 ppm. These spectra are plotted with the same absolute intensity, and the loss factors are calculated by the simulation program. A plot of k vs percent signal loss for a fixed τ is given in Figure 9. The maximum loss is seen when $k = 5 \times 10^4$, or in the intermediate-exchange regime. As the rate increases, the signal begins to grow again as the exchange system goes from the intermediate-exchange to the rapid-exchange limit. The effect of varying the τ value in the echo sequence is shown in Figure 10. Here, k is kept constant at 5×10^4 Hz, and τ is plotted against percent signal loss. Clearly, as τ approaches the rate of exchange, the signal decreases. For a small τ values, <15 μs in this case, the spectrum is not greatly affected (reduced) because the exchange process does not have time to effectively mix the two sites. As τ increases, there is enough time for the sites to completely exchange, and thus the maximum loss is seen. In the fast-exchange limit, a τ value of 10–20 μs might be long enough, relative to k, to allow complete exchange. This exchange, though, will not lead to maximum signal loss, but will cause distortions in the spectrum.

With this is mind, at 95 K the ^{27}Al spectra of alumina surfaces are representative of the slow-exchange regime. Intermediate exchange is seen at room temperature, where we observe the loss

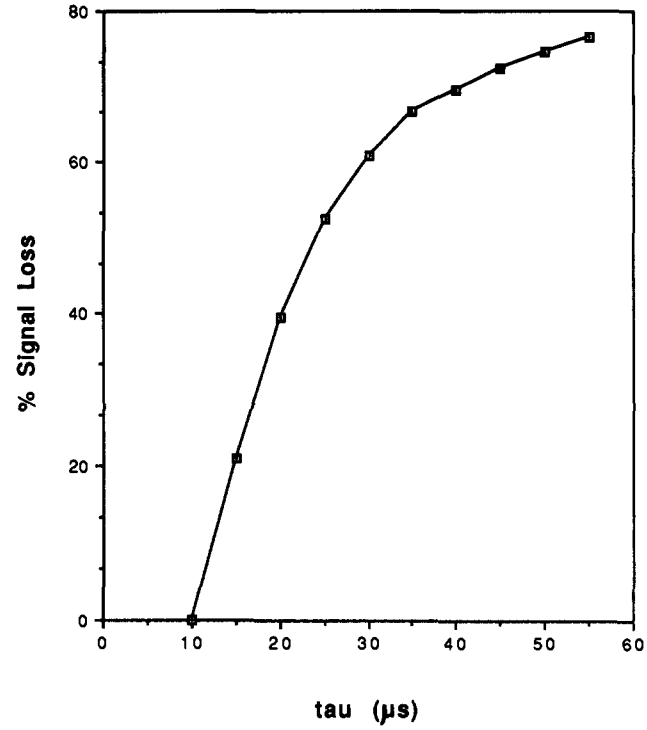

Figure 10. Plot of the percent signal intensity lost when two tensors with Q_{cc} values of 4 and 15 MHz are undergoing exchange at a rate of 5×10^4 vs varying τ values for a spin-echo sequence.

is signal intensity. ^{27}Al experiments were performed in which the temperature was raised to 400 K to determine if some of the signal would be regained. At each temperature up to and including 400 K, there was more of a loss in signal than at 290 K. This implies that we have not yet reached the fast-exchange limit and that at 290 K we may just be entering the intermediate-exchange regime. The results of this experiment point out another potential problem, namely, using the results of a *two*-site exchange system to try to model the results of an *n*-site problem on the surface. Clearly, our results suggest a distribution of reaction rates, chemical shifts, electric field gradients, etc., that are present on the surface. Hence, a broad intermediate-exchange region will be observed as compared to Figure 9.

Partially Dehydroxylated Surfaces. As we have shown, untreated aluminas, whose surfaces are comprised of physisorbed and chemisorbed water, as well as protons, show a decrease in integrated ^{27}Al NMR signal intensity with increase in surface area. Heat-treated, or dehydroxylated, aluminas do not fit into this category as they have no physisorbed water, and thus a significantly reduced population of surface hydroxyls. The ^{27}Al NMR of aluminas which have been dehydroxylated, therefore, should not show effects of any physisorbed water motion (Scheme 1) but only those effects due to the surface site exchange of protons (Schemes 2 and 3). The series of samples PDA, IDA, and EDA are dehydroxylated γ-aluminas produced as described in the Experimental Section. If the broadening at room temperature is partially due to hydroxyls combining with protons or other hydroxyls to form water, followed by the water migrating across but not leaving the surface, then one would expect to see an increase in signal intensity as one goes from untreated γ-alumina to PDA, IDA, and then EDA. This is because as hydroxyl groups are removed, water formation and subsequent migration would decrease, thereby decreasing the effect of the quadrupolar relaxation mechanism and leading to narrower resonances. In fact, what is observed experimentally does not support this idea. All of the dehydroxylated samples have a lower ^{27}Al signal intensity than γ-alumina at both 290 and 90 K. These heat-treated samples do, however, gain intensity among themselves as one goes from PDA to EDA, while they also have comparable gains in intensity from 290 to 90 K relative to the other transition-aluminas studied. These results indicate that all of the sources of the surface dy-

namics have not been removed by the dehydroxylation treatments. Peri[3] found that temperatures of 400 °C would successfully remove all physisorbed water, but not all surface hydroxyl groups, and that aluminas dried above 650 °C would still contain isolated hydroxyl groups. At temperatures above 1000 °C, hydroxyl groups continue to combine and traces of water can still be removed from the alumina surface. Given this, the PDA sample will contain a small population of surface hydroxyls as isolated and perhaps neighboring hydroxyl groups, while the IDA and EDA samples may only have isolated hydroxyl groups present. In the case of the dehydroxylated samples, the second type of dynamics, i.e., proton hopping (Schemes 2 and 3), can be envisioned to occur at a faster rate than on the fully hydroxylated samples which have physisorbed water on the surface. This is because there are more neighboring defect sites into which the protons can move.

It has been suggested that there are different types of defect or strain sites on the surface which are responsible for catalytic activity.[7] The surface strain caused by some sites is larger than from other sites, and it is likely that protons would preferentially move to the more strained sites in order to minimize the strain, and thus the total energy of the system. The protons on the untreated surfaces would have only those defect sites which were produced by the initial heating process used to make the catalytic surfaces in which to move. These surface protons are also in competition with the physisorbed water. The protons remaining on dehydroxylated surfaces would not have their motion as inhibited or constrained but would be able to move about the surface more freely as the hydroxyl population decreases and the number of vacant surface defect sites increases. The population of Lewis acid sites on dehydroxylated surfaces is at least as large as untreated surfaces. As we have seen from MO calculations these types of sites give rise to the largest Q_{cc}'s, thereby broadening the signal more than for the untreated surfaces. Thus, we see an even further decrease in the signal intensity of the dehydroxylated samples vs α-alumina at room temperature than with the untreated γ-alumina due to the increased effect of the surface dynamics as well as the increase in the Lewis acid site population. Dehydroxylation increasing in concert with signal intensity may indicate that since the overall surface hydroxyl population is lowered, the average aluminum atom at the surface does not "feel" the effects of the proton motion as much. Also, the surface area of the dehydroxylated samples decreases from PDA to EDA, giving rise to the same effect as is seen for the untreated transition-aluminas as one goes to lower surface area.

Summary and Conclusions

The history of alumina use in catalytic systems is long-lived. However, the understanding of the reaction mechanisms involved in these systems is still in its infancy. Through the use of variable-temperature solid-state ^{27}Al NMR, we have shown that the surface of transition-aluminas may be described as being dynamic. This study was concerned with lateral surface proton motion, where it was assumed that any interstitial migration of protons would occur at a much slower rate and would not have a significant effect on the ^{27}Al NMR signal. The nature of the lateral surface dynamics is manifested in the mobility of surface protons, which are derived from either physisorbed or chemisorbed water. This motion produces an efficient quadrupolar relaxation pathway and aids in the exchange of one type of surface aluminum with another, which results in a broadened line shape and loss in signal intensity. Because these are surface effects, the ^{27}Al NMR signal intensity decreases with increasing surface area. Lowering the temperature to 90 K significantly reduces surface proton mobility, which is shown as a greater than calculated increase in signal for aluminas other than α-alumina. Such dynamics must, therefore, be accounted for in any formulation of a model of the surface of an alumina.

Acknowledgment. We gratefully acknowledge support from the National Science Foundation via Grants CHE85-44272, CHE86-11306, and CHE89-21632. Further, we acknowledge the efforts of John C. Edwards during the initial stages of this research. We also give Dr. Murray Smigel of Convex Computer Corp. special acknowledgment for his help with the MO calculations described and the generous donation of the needed computer time.

Registry No. Al_2O_3, 1344-28-1.

Selective Shaped Pulse Decoupling in NMR: Homonuclear [^{13}C]Carbonyl Decoupling

M. A. McCoy* and L. Mueller

Contribution from Bristol-Myers Squibb Pharmaceutical Research Institute, P.O. Box 4000, Princeton, New Jersey 08543. *Received June 20, 1991*

Abstract: We introduce a novel pulse sequence that is capable of frequency-selective spin decoupling. This sequence uses radio-frequency pulse shaping to greatly attenuate off-resonance side bands which are inherent in broad-band decoupling sequences but, within the bandwidth of the sequence, retains the quality of decoupling possible with the commonly used WALTZ-16 sequence. Selective carbonyl decoupling is demonstrated in a heteronuclear multiple quantum correlation experiment where it is shown that efficient decoupling of the carbonyl from the Cα carbons occurs without distorting nearby aromatic coherences. Selective decoupling promises to be a powerful new tool in high-resolution spectroscopy and especially in protein NMR where it is possible to remove the effects of undesirable isotopic labels.

In NMR experiments on ^{13}C- and ^{15}N-labeled proteins, the large homonuclear carbonyl coupling to the C_α carbon ($J_{CC} \sim 60$ Hz) and, to a lesser extent, the $^{13}C{=}O$ coupling to ^{15}N ($J_{CN} \sim 15$ Hz) result in splitting that translates to a loss in signal intensity and unnecessarily complicates the frequency spectrum. Refocusing of $^{13}C{=}O$ C_α coupling with frequency-selective inversion pulses can reverse the undesirable evolution of spin coherence at a specific time $t_1/2$ so that after further evolution to time t_1 it appears as if no carbonyl coupling is present.[1] This refocusing requires pulses that are highly frequency selective for both Zeeman and transverse magnetization, which turn out to be

(1) Brüschweiler, R.; Griesinger, C.; Sørensen, O. W.; Ernst, R. R. *J. Magn. Reson.* **1988**, *78*, 178.

0002-7863/92/1514-2108$03.00/0